
MRI-based Visualisation of Orbital Fat Deformation During Eye Motion

Charl P. Botha¹, Thijs de Graaf², Sander Schutte², Ronald Root², Piotr Wielopolski³, Frans C.T. van der Helm², Huibert J. Simonsz⁴, and Frits H. Post¹

¹ Data Visualisation, Delft University of Technology, Delft

² Biomechanical Engineering, Delft University of Technology, Delft

³ Department of Radiology, Erasmus Medical Centre, Rotterdam

⁴ Department of Ophthalmology, Erasmus Medical Centre, Rotterdam
The Netherlands

Summary. Orbital fat, or the fat behind the eye, plays an important role in eye movements. In order to gain a better understanding of orbital fat mobility during eye motion, MRI datasets of the eyes of two healthy subjects were acquired respectively in seven and fourteen different directions of gaze. After semi-automatic rigid registration, the Demons deformable registration algorithm was used to derive time-dependent three-dimensional deformation vector fields from these datasets. Visualisation techniques were applied to these datasets in order to investigate fat mobility in specific regions of interest in the first subject. A qualitative analysis of the first subject showed that in two of the three regions of interest, fat moved half as much as the embedded structures. In other words, when the muscles and the optic nerve that are embedded in the fat move, the fat partly moves along with these structures and partly flows around them. In the second subject, a quantitative analysis was performed which showed a relation between the distance behind the sclera and the extent to which fat moves along with the optic nerve.

1 Introduction

The human eye is able to rotate at up to 1000° per second and has an angular range of 100° horizontally and 90° vertically. It is able to do all of this with almost no translation of its centre. Eye movement is driven by six eye muscles. The left image in Figure 1 shows the medial and lateral rectus muscles that are responsible for horizontal motion. The right image shows the superior and inferior rectus muscles that are responsible for vertical motion. The two oblique eye muscles are able to perform torsionary eye motion, i.e. rotation around the direction of gaze.

The exact nature and parameters of the mechanics supporting eye movement is still not entirely clear. For example, as part of the “Active Pulley

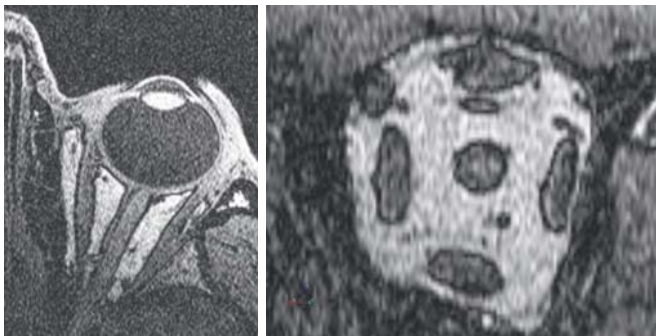


Fig. 1. The left image is of an axial slice of an MRI dataset of an eye showing the medial and lateral rectus muscles and the optic nerve. The white material surrounding the eye-muscles is orbital fat. On the left of the image, part of the nose is visible. The right image shows a slice orthogonal to that, intersecting at the diagonal line shown on the axial slice. This orthogonal slice shows the superior and inferior rectus muscles as well as the superior oblique muscle. The inferior oblique muscle is not visible in this image, but is diagonally opposite to the superior oblique.

Hypothesis”, it was proposed that the connective tissue bands connecting the horizontal rectus muscles to the inside wall of the orbit (eye socket), first described by Tenon in 1816 and later called “pulleys” by Miller in 1989 [Mil89], are responsible for the fact that these muscles show a specific inflection or bending point during vertical eye motion [Dem02].

However, in recent work it was demonstrated with a finite element analysis model of the eye as well as clinical observation that these muscles show this inflection point without any connective tissue structures [SvdBK⁺03, Sch05]. It has also become clear that the orbital fat, i.e. the fat behind the eye, plays an important role in the mechanics of eye movement. Currently, relatively little is known about the mobility of this fat during eye movement.

This paper documents our initial efforts on studying the mobility of the orbital fat during eye movements. Inspired by previous work in this regard [AV02], we applied a deformable registration technique to derive 3-D optical flow fields from two series of MRI datasets of two healthy subjects in different directions of gaze. The resultant 3-D deformation vector fields were used to visualise and measure the motion of orbital eye-fat during eye movement.

Fields resulting from optical flow or deformable registration algorithms are in actual fact displacement fields. However, in keeping with the registration nomenclature we will also refer to them as deformation fields.

Our contribution lies in the fact that this study comes to relevant conclusions about three-dimensional orbital fat mobility during eye motion. These conclusions confirm previous work performed on two-dimensional data and lead to interesting new questions. In addition, we demonstrate that using

interactive advection volumes is an effective way of investigating orbital fat mobility based on 3-D optical flow vector fields derived from MRI.

The rest of this paper is structured as follows: section 2 contains a brief summary of work related to this study. Section 3 explains the methods and tools we used for our study. In section 4 we show the results of our analysis and in section 5 we summarise our findings and indicate avenues for future work.

2 Related Work

There are numerous examples of estimating 3-D motion given a set of volumes. For example, in [dLvL02], block matching is used to derive motion vectors. We have chosen the Demons deformable registration algorithm [Thi96] due to its straight-forward implementation and the fact that it is a proven choice for the non-rigid registration of MRI datasets. However, we do plan to test more optical flow approaches in the future.

In [AV02], the 2-D Lucas and Kanade optical flow algorithm [LK81] is extended to three dimensions and applied to various test datasets as well as an MRI dataset of an eye in different directions of gaze. For reasons mentioned previously, we selected the Demons algorithm. In addition, we make use of advection to quantify the fat motion. Another important difference is that [AV02] focuses more on the validation of the actual technique rather than on the investigation of actual fat mobility. It does come to the conclusion that the orbital fat “deforms like a liquid and less like a solid”. It also describes how the fat fills the area behind the moving optic nerve from above and below during horizontal motion. This is described as “this tissue [the fat], thus, fills the vacuum left by the nerve, as behind a spoon moving through syrup”.

In a previous two-dimensional study based on MRI data, it was determined that the orbital fat surrounding the optic nerve moves horizontally only 54% as much as the optic nerve itself during horizontal eye motion [SHM⁺06].

3 Methods

3.1 Acquisition

MRI volume datasets were acquired of the eyes of two healthy subjects in respectively seven and fourteen different directions of gaze.

For the first subject, T1-weighted scans were acquired on a 1.5 Tesla General Electric MRI scanner. We made use of a mobile transceiver surface coil for higher resolution. This resulted in seven $512 \times 512 \times 84$ MRI datasets with resolution $0.273 \times 0.273 \times 0.5\text{mm}$. For the deformation analysis, four of the datasets were used: the central direction of gaze, and three directions of gaze to the left.



Fig. 2. The acquisition setup. The subject's head has been fixed to the scanning table. The mobile transceiver is visible over the subject's right eye.

For the second subject, T1-weighted scans were acquired on a 3 Tesla General Electric MRI scanner. This resulted in fourteen $512 \times 512 \times 128$ MRI datasets with resolution $0.312 \times 0.58 \times 0.4\text{mm}$. For the deformation analysis, thirteen of these datasets were used: the central direction of gaze, six directions to the left and six to the right.

Figure 2 shows the acquisition setup. The inside of the MRI tube was marked with fixation points at the desired directions of gaze for the subject to focus on during the acquisition.

3.2 Software Tools

The Delft Visualisation and Image processing Development Environment, or DeVIDE, is a software environment for the rapid prototyping and application of visualisation and image processing techniques [Bot04]. It makes use of the VTK [SML99] and ITK [ISNC03] software toolkits. Its primary user interface is a graphical canvas where boxes, representing functional modules or algorithms, can be placed. These boxes can be connected together to form function networks. This is similar to other packages such as OpenDX [AT95] and AVS [UFK⁺89]. What distinguishes DeVIDE is its focus on medical visualisation and image processing, and the extensive interaction facilities made possible by the use of Python [vR01], a very high level dynamically typed language, in the program main loop. All processing and visualisation described in this paper was performed using the DeVIDE software.

3.3 Pre-processing

During image acquisition, the subject's head was fixed to the MRI patient table with surgical tape in order to minimise head motion during the relatively

long total scan duration. Acquisition takes approximately one minute per direction of gaze, but significant time is spent on setup actions between directions of gaze. In spite of the head fixation, slight subject head motion did occur. In order to eliminate this rigid head motion in the acquired data, corresponding sets of six bony landmarks each were defined in all datasets. The datasets representing the central direction of gaze was chosen as the reference. Rigid transformations, optimal in a least squares sense, were derived to map the three other landmark sets onto the reference set [Hor87]. These transformations were used to resample the data volumes with cubic interpolation, thus eliminating most of the rigid motion. All registrations were visually inspected and improved if not satisfactory by re-adjusting the selected landmarks.

As explained in section 3.1, the inside of the MRI tube was marked with fixation points at the desired directions of gaze. However, the desired directions of gaze and the final actual directions of gaze were obviously not equal, as the subjects could focus with either one of their eyes. In order to determine the actual directions of gaze, we started by segmenting the lenses in all datasets and determining the centroids of these segmentations. Segmentation was based on a thresholding and 3-D region growing starting from a user selected marker in the lens. Subsequently a sphere was fitted to the eye in order to find its centre. Figure 3 illustrates this procedure. The vector between the centre of the lens and the centre of the eye determines the direction of gaze. For each of the subjects, one of the datasets was chosen as the reference, or centre direction of gaze.

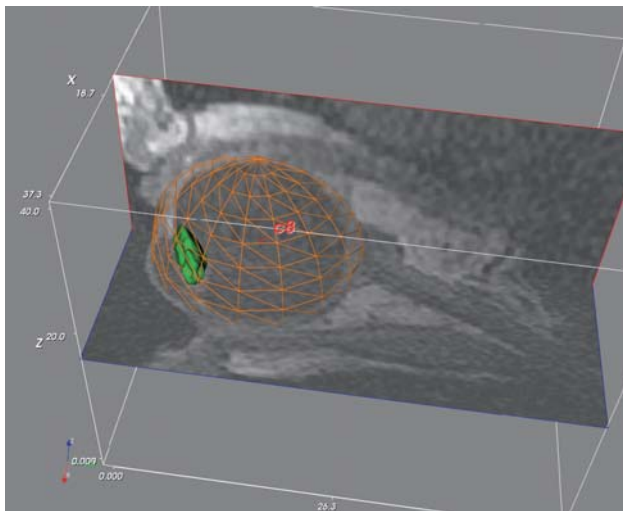


Fig. 3. Procedure for determining the actual directions of gaze. The lens is automatically segmented and its centroid is determined. The actual direction of gaze is determined by this centroid and the centre of the sphere that has been fitted to the eye.

For the first subject we determined the three directions to the left of the centre direction to be respectively 33° , 24° and 14° . For the second subject, the actual directions of gaze were 37.5° , 30.1° , 26.0° , 18.8° , 12.4° , 4.6° to the left of the centre direction, and 7.0° , 12.8° , 18.9° , 25.5° , 32.3° and 38.6° to the right.

3.4 Deformable Registration

The Demons deformable registration algorithm [Thi96] was used to determine the 3-D vector datasets describing the orbital fat deformation from the central direction of gaze through all directions of gaze to its left and to its right. In the case of the first subject, deformation fields were determined from 0° to 14° , from 14° to 24° and from 24° to 33° . For the second subject, fields were determined starting from the central direction to all directions to the left and to the right. The Demons algorithm was chosen due to its straight-forward implementation, and the fact that it is often used for this kind of deformable registration problem. We have also implemented the 3-D version of the Lukas and Kanade optical flow algorithm and as part of our future work plan to compare it with the Demons approach.

Because the Demons algorithm is based on the assumption that corresponding points in the source and target datasets have the same intensity, the intensity values of each pair of datasets were normalised by using a histogram matching implementation from ITK [ISNC03].

3.5 Visualisation and Measurement

The resulting vector fields can be visualised with traditional flow visualisation techniques such as glyphs or streamlines, but these techniques all suffer from the problems plaguing most three-dimensional flow visualisation techniques: occlusion, lack of directional cues, lack of depth cues and visual complexity. To compound matters, we are dealing with time-varying data. In spite of all this, existing techniques are a great help in localising regions of interest that can be examined in more depth with other techniques.

In our case, we were interested in the fat deformation in specific areas. We chose to apply user-guided advection volumes. Small sub-volumes are placed in regions of interest. Each sub-volume is defined by a containing polygonal surface. Points are placed within the interior of this sub-volume at a user-definable density. Each of these points, as well as the vertices defining the containing surface, can then be displaced by the interpolated deformation vectors at their various positions, for that time-step. Figure 4 shows this process for a single time-step and a single spherical volume. The deformed volume, shown on the top right, is used as the initial volume for the next vector field. In this way we can keep on deforming the volume as many times as we have vector datasets.

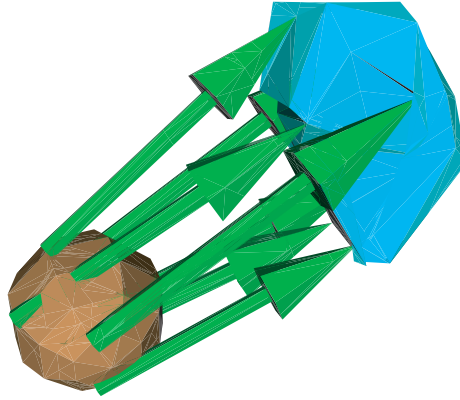


Fig. 4. The sub-volume advection, shown for a single spherical region of interest and for a single time-step. The sphere on the left is the original as selected by the user. The object on the right has been deformed by the current vector field. The vector field associated with the next time step will subsequently be applied to the vertices of the deformed region of interest.

The DeVIDE software allows one to place any number of these volumes in an MRI dataset. As soon as a volume is placed, it is advected through all loaded vector fields and the initial volume as well as all deformed volumes for that point are visualised. An already placed volume can also be moved. This allows for the interactive exploration of a time-varying deformation vector field. Figure 5 shows an example of such an interactive visualisation with four initial volumes advected over 12 vector datasets.

Another important reason to select specific regions of interest is the fact that the deformation field has the highest quality on textured structures embedded in the orbital fat. Similar to the previous 2-D study [SHM⁺06], we experimented by placing advection volumes on vascular structures, preferably on bifurcations.

Results can be visually studied. In addition, similar to the actual direction of gaze determination discussed in section 3.3, the relative direction of a specific advected volume can be determined with regards to the centre of the eye.

4 Results

The two subjects were studied using different methods. The first subject was part of a pilot study, and we qualitatively inspected specific anatomical regions with advection volumes. In the second subject, we quantitatively tracked a number of fat regions chosen specifically on vascular structures in the orbital fat, also using advection volumes.

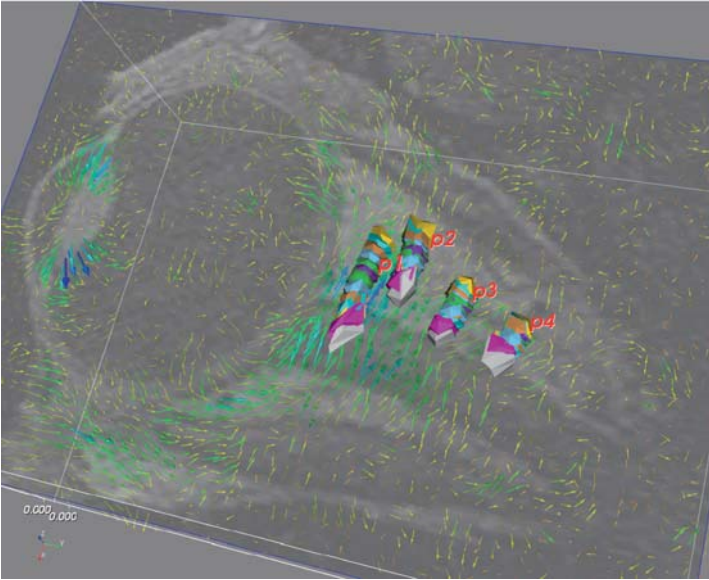


Fig. 5. A visualisation with four advection volumes over 12 time-varying vector fields. The volumes have been chosen in the same plane as the optic nerve, on venous landmarks in order to verify the findings of a previous 2-D study. In each of the four cases, the green sphere in the middle is placed in the centre direction of gaze, and is advected both to the left and to the right.

In the first subject, three regions were selected for closer qualitative inspection:

1. The region between the medial rectus and the eye. As the eye turns anti-clockwise, this muscle “rolls up” onto the eye.
2. Around the optic nerve right behind the eye.
3. The region at the apex where the eye-muscles and optic nerve meet, about 25mm behind the eye.

In all of these regions a number of spherical volumes were placed and advected with the three deformation vector fields. In the first case, i.e. between the medial rectus and the eye, the resolution of the datasets and of the resultant vector fields was too low to make any kind of judgement.

In the second case, seven small spherical volumes were placed directly behind the eye: six surrounding the optic nerve at regular angles and one in the optic nerve itself. As the left eye turns anti-clockwise, the optic nerve moves medially, i.e. in the direction of the nose. The fat surrounding the optic nerve moved in the same direction and primarily transversally. What was significant, is that the fat moved only half as much as the optic nerve.

In the third case, advected volumes indicated that the fat moved primarily in the same direction as the muscles. Once again, the fat moved half as much as the muscles.

In the second subject data, we selected a number of advection volumes specifically on vascular features in the orbital fat. In the first case, four markers were chosen in the same axial plane as the optic nerve in order to confirm the findings of [SHM⁺06]. In that 2-D analysis, a single MRI slice containing the optic nerve was selected for the analysis and markers were manually tracked for all acquired datasets.

In our case, the relative direction of a specific advection volume in any vector field can be determined similarly to the way in which the directions of gaze were determined. Figure 6 shows the relative rotations for each of the four selected volumes over all vector fields. For each advection volume, the linear regression with derived coefficients a and b is shown as well. Our findings, although based on optical flow advection, concur with their manually tracked results. In our case, fat rotation is between 0.35 times and 0.07 times as much as eye rotation for markers with a distance between 3.3mm and 14.0mm behind the eye. In [SHM⁺06], fat rotation at 4mm was 0.36 times as much and at 14.5mm 0.07 times as much as the eye rotation.

We also selected four markers in a plane completely above the optic nerve. Although not as pronounced, there is a clear relation between the distance

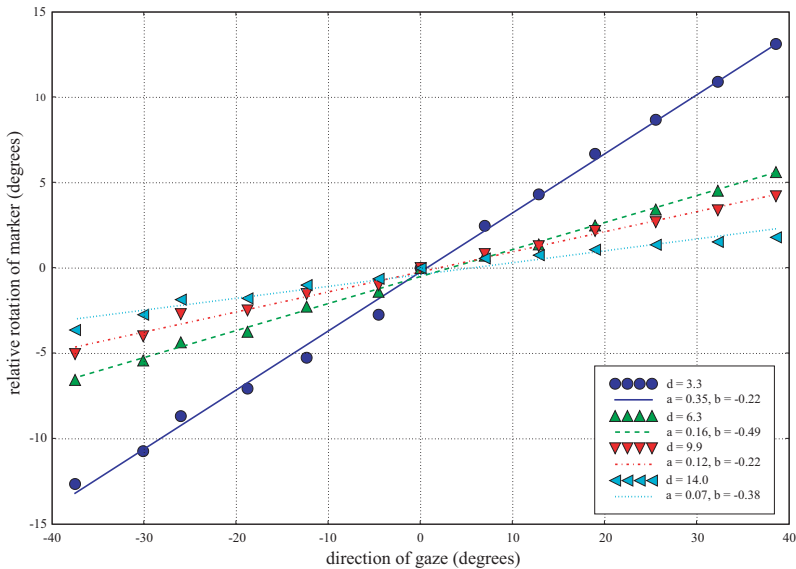


Fig. 6. Relative angles of four advection volumes in an axial slice containing the optic nerve over relative direction of gaze. d refers to the distance behind the eye for that specific advection volume. Also shown is the linear regression derived from this data with coefficients a and b .

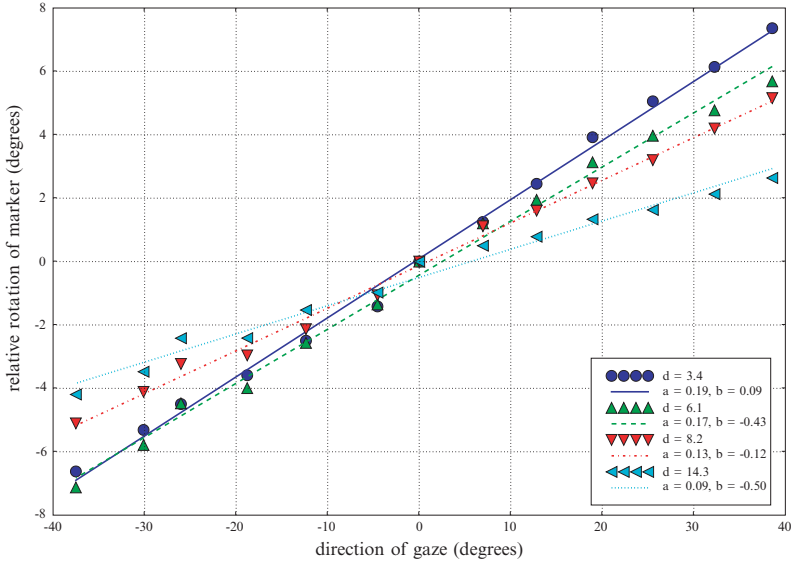


Fig. 7. Relative angles of four advection volumes in an axial slice above the optic nerve over relative direction of gaze. d refers to the distance behind the eye for that specific advection volume. Also shown is the linear regression derived from this data with coefficients a and b .

behind the eye and the ratio of fat rotation to eye rotation. Figure 7 shows the measurements and linear regression for the markers in this plane.

In the third case, we chose a number of vascular markers in random positions around the optic nerve. The relation between distance and rotation ratio is still apparent although far less pronounced. See Figure 8 for the measurements and linear regression results.

5 Conclusions and Future Work

In this paper we have documented an initial study of 3-D orbital fat dynamics based on multiple MRI datasets acquired of a two healthy subjects' eyes during different directions of gaze. Time-varying three-dimensional vector fields were generated by applying the Demons deformable registration technique to pairs of MRI datasets of sequential directions of gaze. These vector fields were visualised with the DeVIDE software system and analysed by making use of advection volumes.

In the first subject it was qualitatively determined that directly behind the eye and at the apex where the muscles and the optic nerve meet, fat moves 50% less than respectively the optic nerve and the muscles embedded in it. In other words, orbital fat moves partly along with these moving structures, but it partly deforms around them as well.

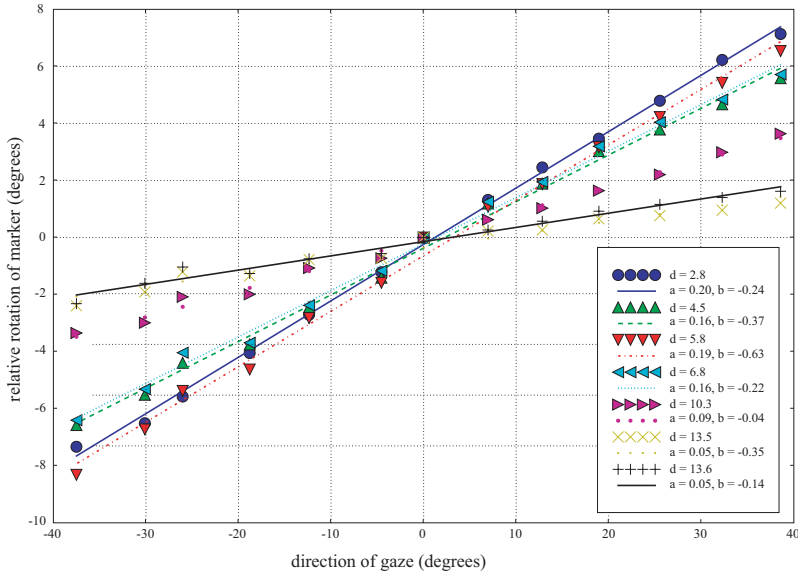


Fig. 8. Relative angles of seven advection volumes randomly selected in vascular features around the optic nerve over relative direction of gaze. d refers to the distance behind the eye for that specific advection volume. Also shown is the linear regression derived from this data with coefficients a and b .

In the second subject, the rotation angles of specific vascular markers were tracked over all thirteen vector fields. For markers in the same plane as the optic nerve, our findings correlated well with the findings of a previous 2-D study of the same data where markers were manually tracked from frame to frame. For markers in a plane above the optic nerve, there was still an apparent inverse relation between the distance from the eye and the ratio between the deformation of the fat and the rotation of the eye itself. For vascular markers randomly chosen all around the optic nerve, the relation was weaker. This is to be expected, as markers further above and below the optic nerve will be less affected by the motion of the optic nerve itself through the fat.

In all cases, motion of the vascular structures, calculated according to the Demons optical flow, was a fraction of the eye rotation. This implies that the optic nerve moves through the fat. In other words, orbital fat has to deform less, which would probably require less energy.

With the Demons algorithm, we could only reliably track textured features, such as the vascular structures, in the fat. We plan to implement more robust 3-D optical flow techniques in order to be able to track a large part of the orbital fat reliably. Subsequently, we will measure advection for a dense sampling of complete orbital fat regions of interest in order to see if our findings still hold.

The interactive advection volumes constitute an effective method to visualise and quantify local fat deformation. However, a more global visualisation technique would be useful to help understand the complex orbital fat deformation fields. One interesting idea is the development of a realistic fluid flow simulation and visualisation that uses the derived vector fields as basis, so that the fat deformation can be studied in pseudo real-time. We will also continue our investigation of alternative techniques for the visualisation of local deformation.

The fixation of the subject's head during scanning has to be improved. The rigid motion can be eliminated as explained in this paper, but it is desirable to minimise head motion during the acquisition phase. For the residual motion that still might occur, it is important to localise easily identifiable rigid landmarks during acquisition. We are currently investigating techniques to improve head fixation and landmark localisation.

Importantly, the approach documented in this paper is based on the acquisition of a series of static scenes. During the acquisition of a particular direction of gaze, the eye is in a state of equilibrium. Due to this, the dynamic behaviour of orbital fat during eye movements, e.g. the viscous or inertial effects, is not captured. In spite of its limitations, our approach still yields valuable information about the 3-D deformation of orbital fat, especially since it is currently not possible to acquire real-time 3-D MRI data of the eye in motion. In future, we will make use of 2-D tagged MRI to study the dynamic behaviour in more detail and integrate these effects into our 3-D model.

References

- [AT95] Greg Abram and Lloyd Treinish. An extended data-flow architecture for data analysis and visualization. In *Proceedings of IEEE Visualization '95*, page 263. IEEE Computer Society, 1995.
- [AV02] Michael D. Abràmoff and Max A. Viergever. Computation and visualization of three-dimensional soft tissue motion in the orbit. *IEEE Transactions on Medical Imaging*, 21(4):296–304, 2002.
- [Bot04] Charl P. Botha. DeVIDE: The Delft Visualisation and Image processing Development Environment. Technical report, Delft Technical University, 2004.
- [Dem02] Joseph L. Demer. The orbital pulley system: a revolution in concepts of orbital anatomy. *Annals of the New York Academy of Sciences*, 956:17–33, 2002.
- [dLvL02] Wim de Leeuw and Robert van Liere. Bm3d: motion estimation in time dependent volume data. In *VIS '02: Proceedings of the conference on Visualization '02*, pages 427–434, Washington, DC, USA, 2002. IEEE Computer Society.
- [Hor87] Berthold K.P. Horn. Closed-form solution of absolute orientation using unit quaternions. *Journal of the Optical Society of America A*, 4:629–642, 1987.

- [ISNC03] Luis Ibanez, Will Schroeder, Lydia Ng, and Joshua Cates. *The ITK Software Guide*. Kitware Inc., 2003.
- [LK81] B. Lucas and T. Kanade. An iterative image registration technique with an application to stereo vision. In *Proc. DARPA Image Understanding Workshop*, pages 121–130, 1981.
- [Mil89] J.M. Miller. Functional anatomy of normal human rectus muscles. *Visual Research*, 29:223–240, 1989.
- [Sch05] Sander Schutte. Orbital mechanics and improvement of strabismus surgery. Master’s thesis, Delft University of Technology, 2005.
- [SHM⁺06] Ivo Schoemaker, Pepijn P W Hoefnagel, Tom J Mastenbroek, Cornelis F Kolff, Sander Schutte, Frans C T van der Helm, Stephen J Picken, Anton F C Gerritsen, Piotr A Wielopolski, Henk Spekreijse, and Huibert J Simonsz. Elasticity, viscosity, and deformation of orbital fat. *Invest Ophthalmol Vis Sci*, 47(11):4819–4826, Nov 2006.
- [SML99] Will Schroeder, Ken Martin, and Bill Lorensen. *The Visualization Toolkit*. Prentice Hall PTR, 2nd edition, 1999.
- [SvdBK⁺03] S.Schutte, S.P.W. van den Bedem, F.van Keulen, F.C. T. van der Helm, and H.J. Simonsz. First application of finite-element (fe) modeling to investigate orbital mechanics. In *Proceedings of the Association for Research in Vision and Ophthalmology (ARVO) Annual Meeting*, 2003.
- [Thi96] J.-P. Thirion. Non-rigid matching using demons. In *Proceedings of IEEE Computer Vision and Pattern Recognition (CVPR)*, pages 245–251, 1996.
- [UFK⁺89] C. Upton, T Faulhaber, D. Kamins, D. Laidlaw, D. Schlegel, J. Vroom, R. Gurwitz, and A. van Dam. The Application Visualization System: A Computational Environment for Scientific Visualization. *IEEE Computer Graphics and Applications*, pages 30–42, July 1989.
- [vR01] Guido van Rossum. *Python Reference Manual*. Python Software Foundation, April, 2001.